Original Article

Magnetic Resonance Imaging Monitoring of Thermal Lesions Produced by Focused Ultrasound

Anastasia Antoniou[1], Nikolas Evripidou[1], Anastasia Nikolaou[1], Andreas Georgiou[1], Marinos Giannakou[1], Antreas Chrysanthou[2], Leonidas Georgiou[2], Cleanthis Ioannides[2], Christakis Damianou[1]*

[1]Department of Electrical Engineering, Computer Engineering and Informatics, Cyprus University of Technology, Limassol, Cyprus, [2]Department of Interventional Radiology, German Oncology Center, Limassol, Cyprus

Abstract

Background: The main goal of the study was to find the magnetic resonance imaging (MRI) parameters that optimize contrast between tissue and thermal lesions produced by focused ultrasound (FUS) using T1-weighted (T1-W) and T2-weighted (T2-W) fast spin echo (FSE) sequences. **Methods:** FUS sonications were performed in *ex vivo* porcine tissue using a single-element FUS transducer of 2.6 MHz in 1.5 and 3 T MRI scanners. The difference in relaxation times as well as the impact of critical MRI parameters on the resultant contrast-to-noise ratio (CNR) between coagulated and normal tissues were assessed. Discrete and overlapping lesions were inflicted in tissue with simultaneous acquisition of T2-W FSE images. **Results:** FUS lesions are characterized by lower relaxation times than intact porcine tissue. CNR values above 80 were sufficient for proper lesion visualization. For T1-W imaging, repetition time values close to 1500 ms were considered optimum for obtaining sufficiently high CNR at the minimum time cost. Echo time values close to 50 ms offered the maximum lesion contrast in T2-W FSE imaging. Monitoring of acute FUS lesions during grid sonications was performed successfully. Lesions appeared as hypointense spots with excellent contrast from surrounding tissue. **Conclusion:** MRI monitoring of signal intensity changes during FUS sonication in grid patterns using optimized sequence parameters can provide useful information about lesion progression and the success of ablation. This preliminary study demonstrated the feasibility of the proposed monitoring method in *ex vivo* porcine tissue and should be supported by *in vivo* studies to assess its clinical potential.

Keywords: Contrast, lesion, monitoring, magnetic resonance imaging, porcine, ultrasound

Introduction

In the last decades, the adoption of thermal ablation modalities has been rapid, enabling safe and efficient delivery of thermal energy to deep-seated body targets.[1,2] This is achieved in a minimally invasive manner with the use of radiofrequency ablation (RFA), microwave ablation (MWA), and laser interstitial thermal therapy (LITT) or in a noninvasive manner using thermal focused ultrasound (FUS).[1,2] While these modalities have been characterized by remarkable developments, such as the introduction of image guidance and robotics,[3,4] the establishment of methods for monitoring ablation lesions has fallen behind.

The superior performance of magnetic resonance imaging (MRI) over other imaging modalities in the acquisition of high-resolution anatomical images with excellent contrast among soft tissues and its ability to monitor tissue temperature noninvasively contributed to developing safe and efficient thermal ablation applications that were more easily adopted into clinical practice.[5,6] Nowadays, there exists a wide range of MRI contrast mechanisms for postsonication lesion assessment and temperature estimation methods, among which MR thermometry based on the proton resonance frequency shift method is predominantly utilized for the intraprocedural monitoring of ablation therapy.[7,8]

The benefits of MRI have been exploited in the context of MWA and RFA for treatment planning and postablation lesion

Received: 11-09-2023 **Revised:** 14-10-2023 **Accepted:** 22-11-2023 **Available Online:** 26-02-2024

Access this article online

Quick Response Code:

Website: https://journals.lww.com/jmut

DOI: 10.4103/jmu.jmu_112_23

Address for correspondence: Dr. Christakis Damianou, Department of Electrical Engineering, Computer Engineering and Informatics, Cyprus University of Technology, 30 Archbishop Kyprianou Street, Limassol 3036, Cyprus.
E-mail: christakis.damianou@cut.ac.cy

How to cite this article: Antoniou A, Evripidou N, Nikolaou A, Georgiou A, Giannakou M, Chrysanthou A, *et al*. Magnetic resonance imaging monitoring of thermal lesions produced by focused ultrasound. J Med Ultrasound 2024;32:297-308.

assessment.[9-11] As an example regarding treatment planning, MRI was employed in the process of US-guided MWA of hepatocellular carcinoma at challenging locations to facilitate tumor selection based on specific safety criteria.[11] Regarding posttreatment evaluation, it is worth noting that late gadolinium enhancement (LGE) MRI has been proven a feasible method for visualizing RFA-induced lesions and has already been translated in the clinical setting for assessing lesion creation and ablation gaps in atrial thermal ablation.[9,10]

As early as the 1990s, T2-weighted (T2-W) MR sequences were proven to provide excellent contrast between FUS lesions and the surrounding intact tissue in excised and *in vivo* animal tissue,[12-14] and they are still considered among the standard methods for determining the extent of ablation lesions. In the same period, Hynynen *et al*.[15] reported that the size of lesions inflicted in rabbit thigh muscle as visualized on T2-W images matched well the size estimated after tissue excision by caliper measurements and hematoxylin and eosin examination. Another important observation made was that contrast-enhanced T2-W fast spin echo (FSE) imaging showed signal enhancement only in normal tissue and not in lesions.[15] This phenomenon was also reported a few years later for rabbit skeletal muscle,[16] rabbit brain,[17] and synovial tissue[18] and is considered to be attributed to vascular disruption.

Contrast-enhanced T1-weighted (T1-W) FSE imaging also allowed accurate lesion assessment following FUS ablation in rabbit skeletal muscle[16] and brain,[19] synovial tissue,[18] as well as in the clinical setting,[20] where the predicted size was well correlated with the histological lesion size. While both T2-W FSE and contrast-enhanced T1-W FSE sequences are currently considered gold standard for assessing the extent of FUS damage, it seems that in early studies, T1-W FSE sequences were more frequently employed for MR thermometry rather than lesion assessment due to the superior T2-W FSE contrast between intact and damaged tissues reported in numerous studies at the time.[21] Later, it was clarified that the selection of proper sequence in terms of optimizing lesion contrast and delineation highly depends on the specific tissue characteristics. This has been demonstrated in a study by Damianou *et al*.,[22] who performed FUS ablations below and above the boiling level in freshly excised lamb and *in vivo* rabbit tissue. Both T1-W and T2-W FSE imaging were suggested by authors for accurately visualizing ablation lesions in the kidney and liver, whereas for boiling lesions, the T2-W sequence was considered optimal. T1-W FSE imaging was proposed as the optimal sequence for detecting brain lesions of either kind. This was supported by another study where T2-W FSE images showed higher anatomical resolution in the brain compared to T1-W FSE images, but the latter ones offered better contrast between lesion and brain tissue.[23]

Lesion discrimination can be further optimized by selecting proper imaging parameters. For these two basic sequences, T1-W and T2-W FSE, the effect of the repetition time (TR) and echo time (TE) on the resultant contrast-to-noise ratio (CNR) was investigated in excised lamb brain, with authors suggesting the use of TR values above 500 ms and TE values in the range of 40–60 ms for optimized contrast.[23] Another example is a study concerning MR characterization of acute RFA lesions,[24] where TI relaxation times in the range of 500–600 ms were deemed to offer adequate visualization of RFA-induced lesions on LGE images.

Intraoperative monitoring of thermal ablation procedures is critical in deciding whether heating should be continued or modified depending on the desired therapeutic outcome. Lesion monitoring is typically carried out utilizing thermosensitive sequences that allow precise monitoring of temperature evolution for controlled coagulative necrosis.[7,25] There is though a limited literature on the intraprocedural monitoring of signal and contrast changes in the region of interest (ROI) and how these correlate with histological tissue damage and lesion formation.

Bremer *et al*.[26] investigated the efficacy of nonenhanced MRI to accurately monitor lesion size during LITT in pig liver compared to histological size assessment. For this purpose, T1-W turbo fast low-angle shot (FLASH) images were acquired at 1-min interval, revealing a stable reduction in the standardized signal intensity (SI) in the center and periphery of the lesion during LITT, which was partially recovered throughout the cooling period. Furthermore, the SI in the lesion center was found to decrease with increasing deposited laser energy. The employed sequence highly overestimated the lesion size both during and immediately after ablation, whereas after tissue cooling, the visualized damaged area was more accurately associated with the real necrotic area, most probably owing to the absence of temperature-dependent SI fluctuations.[26]

Vergara *et al*.[27] developed a novel system for navigating electrophysiology catheters to ablate atrial tissue under real-time guidance in a 3T MR scanner with the assistance of dedicated MR sequences,[27] whose performance was tested in pigs. Multiple T2-W half-Fourier single-shot turbo spin echo scans were taken during RFA in the myocardium allowing visualization of lesion progression over time. Tissue enhancement observed during and a few minutes after sonication was associated with heat-induced tissue edema and injury, simultaneously providing evidence of lesion creation, which was then confirmed by LGE imaging. As discussed by the authors, the specific sequence tends to overstate the size of the lesion during tissue coagulation by displaying the surrounding edema.[27]

Another study in the content of electrophysiology aimed to establish MRI techniques for intraprocedural lesion visualization. In a study,[28] catheter RFA of myocardial tissues was performed in minipigs. The performance of several MR sequences, including nonenhanced T2-W and contrast-enhanced T1-W gradient echo (GRE), T2-W turbo spin echo (TSE), and FLASH sequences, was tested in terms of acute lesion assessment. The authors proposed nonenhanced

T2-W imaging techniques as beneficial for intraprocedural lesion monitoring because they can be used repeatedly without delays related to the administration of contrast agents. Notably, T2-W images revealed a constant lesion size for the first few hours after RFA.[28]

Clinical results on intraprocedural lesion monitoring during MWA of liver malignancies under MRI guidance in a 1.5 T scanner were reported by Lin *et al*.[29] Specifically, a series of T2-W fat-suppressed fast-recovery FSE images were acquired every 35 s during ablation to monitor tissue effects, with the results showing a gradual SI decrease in the tumor.

In the case of thermal FUS, ultrasonic waves are strongly concentrated resulting in a focal point in the order of a few mm, thus rapidly raising the local tissue temperature to ablative levels without harming nearby tissues.[30] Since the ROI is typically in the order of centimeters, multiple adjacent lesions should be produced to ablate the full ROI volume. Accordingly, remote navigation of the FUS transducer is required for thermal applications in the MRI setting and is achieved with the use of MRI-compatible robotics.[4,31-38]

According to the literature, T1-W and T2-W FSE imaging were mostly employed before FUS ablation for ROI definition and treatment planning and postablation for assessing FUS-induced tissue damage.[8,22,23] Furthermore, they were employed in numerous studies involving the use of tissue-mimicking phantoms and freshly excised animal tissue in the effort to investigate the effect of acoustic energy and grid parameters in the formation of discrete and overlapping lesions, as well as how the selected imaging parameters affect lesion visualization.[22,23] Despite the widespread use of these imaging sequences in MRI-guided FUS studies, their performance was not well investigated in the context of intraoperative lesion monitoring, which may refer to visualization and/or quantification of progressive changes in the SI of the exposed ROI over time and also to real-time monitoring of lesions' formation according to the desired pattern.

Although intraoperative T1-W and T2-W MRI were proven less effective in predicting the therapeutic outcome in terms of the final size of thermal lesions and the extent of tissue necrosis,[39] such monitoring could be beneficial in providing early indication of successful tissue ablation and whether the location of inflicted lesions coincides with the planned ablation patterns, and may also reveal other useful information, such as off-target heat accumulation or insufficient target heating, which are likely to contribute in optimizing the therapeutic outcome and preventing adverse events by enabling intraprocedural alteration of the treatment parameters.

The main goal of the current study was to provide insights on the topic of intraoperative lesion monitoring by presenting indicative results of a series of MRI-guided ablation experiments carried out in freshly excised pork tissue. Multiple sonications in sequential patterns were planned on a custom-made dedicated software and executed by an MRI-compatible robotic system featuring a single-element spherically FUS transducer with a central frequency of 2.6 MHz.[40] The T1 and T2 relaxation times of the pork tissue and coagulation lesion were estimated in a 3 T MRI scanner. The impact of critical imaging parameters on the resultant CNR between coagulated and intact tissues was then investigated to optimize lesion discrimination on T2-W FSE images. Both discrete and overlapping lesions were inflicted in pork tissue samples with simultaneous acquisition of T2-W images at a specific rate to enable visualization of the heated area and assessment of lesion progression with time. Following MRI assessment, the tissue was dissected to confirm successful lesion formation and assess how it is correlated with the CNR changes observed intraoperatively, as well as to obtain quantitative information of the real extent of tissue damage by caliper measurements.

Materials and Methods

This is a preliminary study designed to examine the feasibility of the proposed method of monitoring the progression of FUS lesions by MRI in *ex vivo* porcine tissue. No human or animal participants were involved. Therefore, no informed consent or ethical approval was necessary.

Focused ultrasound ablation of *ex vivo* porcine tissue

FUS was generated by a spherically focused ultrasonic transducer (Piezo Hannas Tech Co. Ltd., Wuhan, China) with a nominal frequency of 2.6 MHz, a diameter of 50 mm, a radius of curvature of 65 mm, and an acoustic efficiency of 30%, which was utilized over the course of all experiments. The transducer was mounted on an MRI-compatible computer-controlled positioning system with 4 degrees of freedom driven by piezoelectric motors, which is detailed described elsewhere,[40] and was supplied by an RF amplifier (AG1016, AG Series Amplifier, T and C Power Conversion, Inc., Rochester, US).

All the experiments were carried out in a General Electric (GE) 1.5 T MRI scanner (GE Signa HD16, GE Healthcare, Chicago, Illinois, United States), as well as in a Siemens 3 T scanner (Magnetom Vida, Siemens Healthineers, Erlangen, Germany). As shown in the photo of Figure 1a, the FUS positioning system was seated on the MRI table and connected to the electronic driving system placed outside of the room through shielded cables. The top cover of the device includes an acoustic opening above the working space of the FUS transducer, to which the porcine tissue sample was fixed. The distance between the bottom surface of the tissue sample and the transducer was adjusted at 35 mm resulting in a focal depth of 30 mm. Degassed, deionized water was poured inside the container until it reached the bottom surface of the tissue sample to achieve efficient ultrasonic coupling. Multichannel body coils (12-channel body coil, Signa 1.5T, GE Healthcare Coils, Aurora, Ohio, USA, and 18-channel body coil, Siemens Healthineers) were utilized for image acquisition. In each case, the coil was attached to a rigid plastic structure at some distance from the tissue surface to improve the signal by preventing

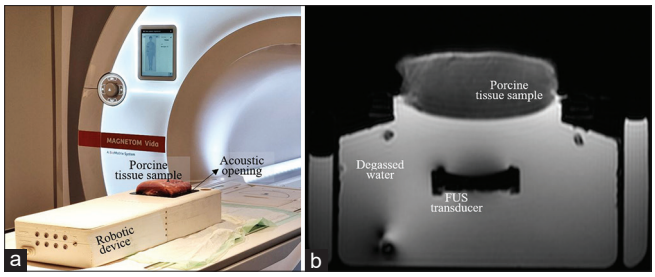

Figure 1: (a) The robotic device positioned on the magnetic resonance imaging (MRI) table with the piece of raw porcine meat mounted on the acoustic opening for ablation experiments in the MRI setting. (b) Axial T2-weighted fast spin echo image (repetition time = 2500 ms, echo time = 90 ms, flip angle = 90°, echo train length = 60, pixel bandwidth = 0.50 Hz/pixel, number of averages = 2, matrix size = 192 × 128, and field of view = 260 mm × 260 mm × 10 mm) of the setup showing the concept of tissue sample placement above the focused ultrasound transducer

tissue vibrations due to FUS from being transferred to the coil.[41] Figure 1b is an axial T2-W FSE image of the setup showing the concept of tissue sample placement above the FUS transducer and through-water ultrasonic coupling. The imaging parameters were as follows: TR = 2500 ms, TE = 90 ms, flip angle (FA) = 90º, echo train length (ETL) = 60, pixel bandwidth (pBW) = 0.50 Hz/pixel, number of averages (NEX) = 2, matrix size = 192 × 128, and field of view (FOV) = 260 mm × 260 mm × 10 mm.

A treatment planning/monitoring software was interfaced with the amplifier and electronic driving system enabling remote control of the motion and ultrasonic parameters. The transducer's location was registered relative to the target location based on images obtained at the level of the porcine tissue sample and transducer, as illustrated in the graphic of Figure 2. Specifically, the user segments the transducer (lower image) and the center of the transducer is fused in the tissue image (upper image). Then, the position of the transducer relative to the tissue is easily found.

Estimation of magnetic resonance relaxation times of lesion and normal porcine tissue

The difference in relaxation times between coagulated and intact porcine tissues was investigated in the 3 T scanner. A piece of raw porcine meat received a single sonication at electrical power of 225 W (corresponding to an acoustic power of nearly 68 W) for 120 s at a focal depth of 30 mm, which resulted in a well-defined lesion. For T1 relaxation time measurements, images of the tissue sample with the inflicted lesion were acquired using a GRE sequence with variable FA. Circular ROIs were defined in the inflicted lesion and surrounding intact tissue. The mean SI measured in each ROI was plotted as a function of FA and the data were fitted to the following formula:[42]

$$M_z = M_{0z}\left(\frac{1-e^{-\frac{TR}{T1}}}{1-\cos a\, e^{-\frac{TR}{T1}}}\right)\sin a \quad (1)$$

where M_z is the longitudinal magnetization, M_{0z} is the magnetization at thermal equilibrium, α is the excitation flip

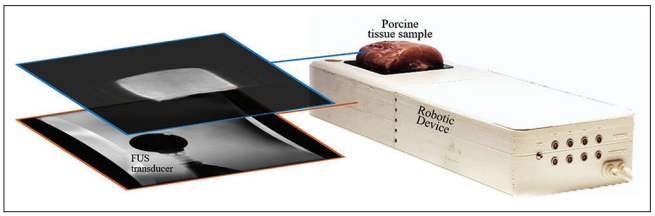

Figure 2: The concept of registering the transducer location relative to the tissue sample by acquiring parallel coronal images at the level of the tissue and transducer

angle (herein referred to as FA), TR is the repetition time, and T1 is the longitudinal relaxation time. The imaging parameters were as follows: TR = 15 ms, TE = 2.3 ms, pBW = 275 Hz/pixel, matrix size = 256 × 256, FOV = 160 mm × 160 mm × 5 mm, NEX = 1, ETL = 1, and FA values ranging from 5º to 26º (step of 3º).

Images were then acquired using a T2-W SE sequence at variable TE for T2 relaxation time mapping. For each ROI, the mean SI was plotted as a function of TE. Following regression analysis, an exponential trendline was fitted to the plotted data to calculate the T2 relaxation time based on the following exponential function:[43]

$$M_{xy} = M_o e^{-\frac{TE}{T2}} \quad (2)$$

describing the recovery of the transverse magnetization M_{xy} following the RF pulse to its initial maximum value of M_o. For image acquisition, the following parameters were employed: TR = 2000 ms, FA = 180°, ETL = 10, pBW = 202 Hz/pixel, matrix size = 192 × 192, FOV = 220 mm × 220 mm × 5 mm, NEX = 1, and TE values ranging from 10 to 110 ms (step of 10 ms).

Effect of magnetic resonance parameters on contrast-to-noise ratio between lesion and normal porcine tissue

In this experimental part, the contrast between the lesion (68 W acoustic power for 120 s) and the surrounding intact tissue was calculated as a function of critical MR parameters in the Siemens 3T MRI scanner for optimizing lesion contrast and detectability on FSE sequences, alternatively referred to as TSE by Siemens.

The effect of TE and ETL on the CNR was explored for the T2-W FSE sequence. Specifically, the ETL was varied from 6 to 129 with a TE equal to 51 ms and the TE was varied from 10 to 154 ms for a contrast ETL of 60, while in both cases, the TR was set at 2000 ms. For the T1-W FSE sequence, variable ETL of 6–129 at a constant TR of 2000 ms and variable TR values of 700–2500 ms at a constant ETL of 60 were tested using a TE of 10 ms. In all cases, the rest imaging parameters were as follows: FA = 180°, pBW = 150 Hz/pixel, matrix size = 256 × 256, and FOV = 280 mm × 280 mm × 5 mm. For comparison purposes, measurements of the CNR between coagulated and intact porcine tissues as a function of TE were also conducted in the GE 1.5 T MRI scanner (TE = 10–150 ms, TR = 2000 ms, FA = 90°,

ETL = 12, pBW = 81.4 Hz/pixel, matrix size = 224 × 192, and FOV = 260 mm × 260 mm × 4 mm).

For both sequences, the changes in CNR with varying matrix sizes and NEX were investigated. Different matrix sizes of 64 × 64, 96 × 96, 128 × 128, 256 × 256, and 512 × 512 were tested using a constant NEX of 1. The NEX was varied from 1 to 4 for a contrast matrix size of 256 × 256. The rest imaging parameters of the T1-W FSE sequence were as follows: TE = 10 ms, TR = 1500 ms, ETL = 60, FA = 180°, pBW = 150 Hz/pixel, and FOV = 280 mm × 280 mm × 5 mm. For T2-W FSE imaging, the TE value was changed to 51 ms and the TR value to 2000 ms.

Circular ROIs of 3 mm in diameter were initially defined for the lesion, normal tissue, and background noise. These ROIs were consistently placed at the same anterior-posterior location to eliminate signal difference due to the drop of signal as one moves further away from the coil. For the CNR estimation, the following formula was used:[44]

$$CNR = \frac{SI_{\text{intact tissue}} - SI_{\text{lesion}}}{\sigma_{\text{noise}}} \quad (3)$$

The SI was measured as the mean value in the corresponding ROI and the σ_{noise} as the standard deviation from a ROI placed in air/background noise, where the noise was assumed to follow a Gaussian distribution.

Lesion monitoring during grid ablation in *ex vivo* porcine tissue

The transducer's location relative to the target was registered in the MRI coordinates and different sonication patterns were planned on the relevant software as described previously. The sonication patterns were executed by the FUS robotic system under MRI monitoring of lesion formation. Specifically, an image was acquired immediately after each individual sonication to visualize lesion progression in discrete and overlapping patterns.

Regarding experiments in the 1.5 T MRI scanner, grid sonications with different spatial steps were performed, where an electrical power of 180 W (acoustical power of 54 W) was applied to each individual grid spot for a total duration of 120 s. T2-W FSE images were acquired using TR = 2000 ms, TE = 59 ms, FA = 90°, ETL = 60, pBW = 27.1 Hertz/pixel, matrix size = 224 × 192, and FOV = 260 mm × 260 mm × 6 mm. The time delay between successive sonications was set at 60 s to minimize prefocal heating.[45]

Accordingly, in the 3 T scanner, T2-W FSE images were obtained with TR = 2500 ms, TE = 48 ms, ETL = 60, FA = 180°, pBW = 50 Hz/pixel, matrix size = 256 × 256, and FOV = 200 mm × 200 mm × 10 mm. Various sonication patterns were tested using a specific electric power of 150 W (acoustic power of 60 W) while the sonication time and spatial step were varied. Again a 60-s cooling time was left between sonications. Postablation, the tissue samples were dissected to visualize and quantify the extent of necrosis in planes parallel and perpendicular to the FUS beam direction.

Results

Estimation of magnetic resonance relaxation times of lesion and normal porcine tissue

The T1 and T2 relaxation times calculated for the lesion and normal porcine tissue are summarized in Table 1. The FUS lesion is characterized by lower relaxation times than the intact tissue, which is considered to be attributed to changes in the water content of coagulated tissue. The difference in these properties between coagulated and intact tissues allowed the assessment of lesion formation by T1-W and T2-W FSE imaging.

Effect of magnetic resonance parameters on contrast-to-noise ratio between lesion and normal porcine tissue

Figures 3 and 4 show the T1-W FSE CNR between lesion (created using 68 W acoustic power and 120-s sonication time) and surrounding intact porcine tissue as well as the ratio of the CNR to the acquisition time plotted against the ETL and TR, respectively. ETL values up to 60 provided CNR higher than 80 allowing proper lesion discrimination [Figure 3]. ETL values in the range of 35–60 resulted in the highest CNR/acquisition time. Considering the importance of minimizing imaging time, an ETL value around 60 was considered optimum.

As shown in the graph of Figure 4, the CNR/acquisition time reached its maximum value and remained almost constant

Table 1: The mean value and standard deviation of the T1 and T2 relaxation times of the lesion and normal porcine tissue at 3 T

Tissue	T1±SD (ms)	T2±SD (ms)
Lesion	738±46	43±3
Porcine tissue	1158±58	50±2

SD: Standard deviation

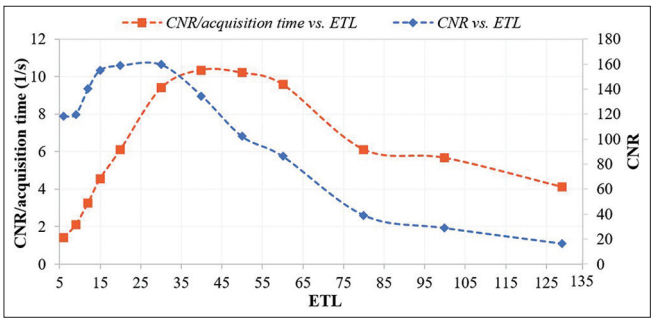

Figure 3: Plots of the contrast-to-noise ratio (CNR) between lesion and normal tissue and CNR/acquisition time of T1-W fast spin echo images (repetition time = 2000 ms, echo time = 10 ms, flip angle = 180°, pixel bandwidth = 150 Hz/pixel, matrix size = 256 × 256, and field of view = 280 mm × 280 mm × 5 mm) versus echo train length (6–129) at 3 T

for TR values in the range of 1500–2000 while the CNR was increased from 90 to 120. Although the TR of 2500 ms may be considered ideal in terms of maximizing contrast, one should alternatively select a value close to 1500 that still provides good CNR (>80) at the minimum time cost possible.

The corresponding results of the ETL and TE effect on lesion contrast of T2-W FSE images are, respectively, shown in Figures 5 and 6. From Figure 5, it is observed that ETL values around 90 resulted in the highest values of CNR/acquisition time but in a very poor CNR (<80), which made lesion detectability difficult. On the contrary, values in the range of 25–60 offered both sufficiently high CNR (>80) and CNR/acquisition time, with the ETL of 60 considered the ideal in terms of minimizing the acquisition time.

In Figure 6, the trend of CNR versus TE increases until the TE of 50 ms and then gradually decreases, clearly suggesting the TE value of 50 ms as optimum for maximizing CNR. Note that the acquisition time is not considered in that case since it is not affected by TE. The corresponding plot for evaluation at 1.5 T shows a quite similar trend but with a lower increase rate in the TE range of 20–90 ms and remarkably smaller CNR values.

The graphs of Figure 7 show the changes in the CNR and CNR/acquisition time of T2-W FSE images as a function of NEX. The minimum NEX of 1 offered CNR much higher than the minimum suggested value of 80, and thus, the use of a larger NEX is unnecessary, provided that it results in longer acquisition times. Similar results were obtained for the T1-W FSE imaging, suggesting the NEX of 1 as the optimum.

Finally, concerning the effect of the matrix size, the CNR decreased from about 740 to 95 with increasing matrix size from 64 × 64 to 512 × 512 for the T1-W FSE imaging, whereas the CNR in T2-W images decreased from 880 to 140. The smallest matrix size is preferred in terms of minimizing the acquisition time, but it provided poor resolution. On the contrary, the biggest matrix size provided excellent resolution and sufficiently high CNR (>80) but at the cost of increased acquisition time. By balancing the

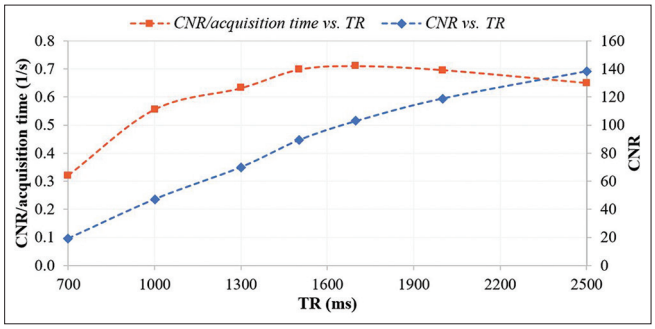

Figure 4: Plots of the contrast-to-noise ratio (CNR) between lesion and normal tissue and CNR/acquisition time of T1-W fast spin echo images (echo train length = 60, echo time = 10 ms, flip angle = 180°, pixel bandwidth = 150 Hz/pixel, matrix size = 256 × 256, and field of view = 280 mm × 280 mm × 5 mm) versus repetition time (700–2500 ms) at 3 T

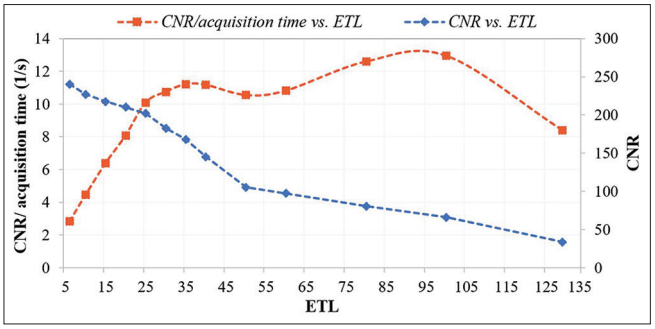

Figure 5: Plots of the contrast-to-noise ratio (CNR) between lesion and normal tissue and CNR/acquisition time of T2-weighted fast spin echo images (repetition time = 2000 ms, echo time = 51 ms, flip angle = 180°, pixel bandwidth = 150 Hz/pixel, matrix size = 256 × 256, and field of view = 280 mm × 280 mm × 5 mm) versus echo train length (6–129) at 3 T

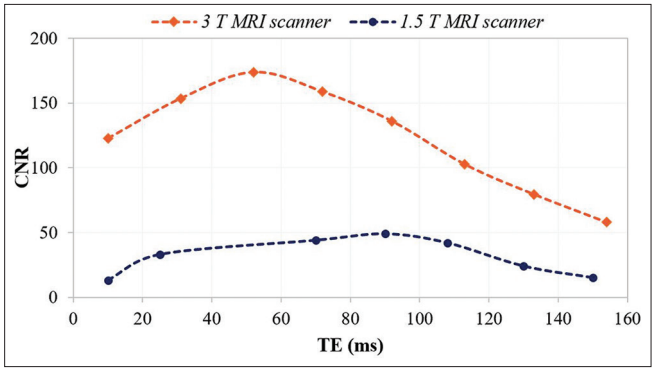

Figure 6: Plots of the contrast-to-noise ratio (CNR) between lesion and normal tissue of T2-weighted fast spin echo images (repetition time = 2000 ms, echo train length = 60, flip angle = 180°, pixel bandwidth = 150 Hz/pixel, matrix size = 256 × 256, and field of view = 280 mm × 280 × 5 mm) versus echo time (10–154 ms) at 1.5 T and 3 T

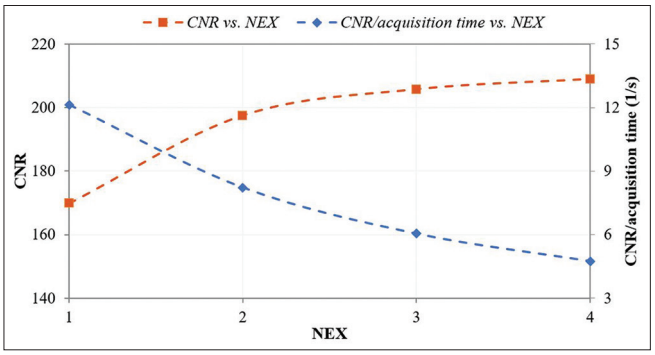

Figure 7: Plots of the contrast-to-noise ratio (CNR) between lesion and normal tissue and CNR/acquisition time of T2-weighted fast spin echo images (repetition time = 2000 ms, echo time = 51 ms, flip angle = 180°, pixel bandwidth = 150 Hz/pixel, matrix size = 256 × 256, and field of view = 280 mm × 280 mm × 5 mm) versus number of averages (1–4) at 3 T

parameters of CNR and imaging time, the use of a 256 × 256 matrix size is proposed.

The MR parameters suggested by the current study for optimizing the CNR between FUS lesions and surrounding tissue on T1-W and T2-W FSE images also considering the importance of minimizing the acquisition time are summarized in Table 2.

Table 2: Summary of the suggested magnetic resonance parameters for optimizing contrast-to-noise ratio between lesion and tissue at the minimum time cost for the specific parameters employed in the study (3 T)

MR parameter	T1-W FSE	T2-W FSE
TR (ms)	1500	2000
TE (ms)	10	50
ETL	60	60
NEX	1	1
pBW (Hz/pixel)	150	150
Matrix size	256×256	256×256
FOV (mm^2)	280×280	280×280
Slice thickness (mm)	5	5

FSE: Fast spin echo, TR: Repetition time, TE: Echo time, ETL: Echo train length, NEX: Number of averages, FOV: Field of view, pBW: Pixel bandwidth, T1-W: T1-weighted, T2-W: T2-weighted, MR: Magnetic resonance

Lesion monitoring during grid ablation in *ex vivo* porcine tissue

An indicative example of lesion monitoring in the 1.5 T MRI scanner is shown in Figure 8. Figure 8a shows a series of T2-W FSE images acquired during ablation in a 3 × 3 pattern with a special step of 10 mm, where the coagulated regions appear as spots of reduced SI. The acoustical power of 54 W applied for 120 s was sufficient to induce well-defined easily detectable lesions. Note that the lesion created at the reference location of the transducer is visible on the left side of all images. Note also that a circular area of reduced intensity appears immediately after the first sonication (#1) but not in the next images, thus revealing heat accumulation in the ROI but no evidence of lesion formation. Figure 8b is a cross-section photo of the meat at 10 mm from the sonicated surface. In contrast to the MRI images, all nine lesions were visible. Tissue was also dissected vertically to visualize the extent of necrosis in a plane parallel to the beam direction. Again, all nine lesions were visible extending 29–32 mm from the tissue top surface, as shown in Figure 8c-e.

Typical results obtained in the 3T MRI scanner are presented in Figures 9-11. All lesions were formed using acoustic power of 60 W. Figure 9 shows T2-W FSE images of the porcine tissue

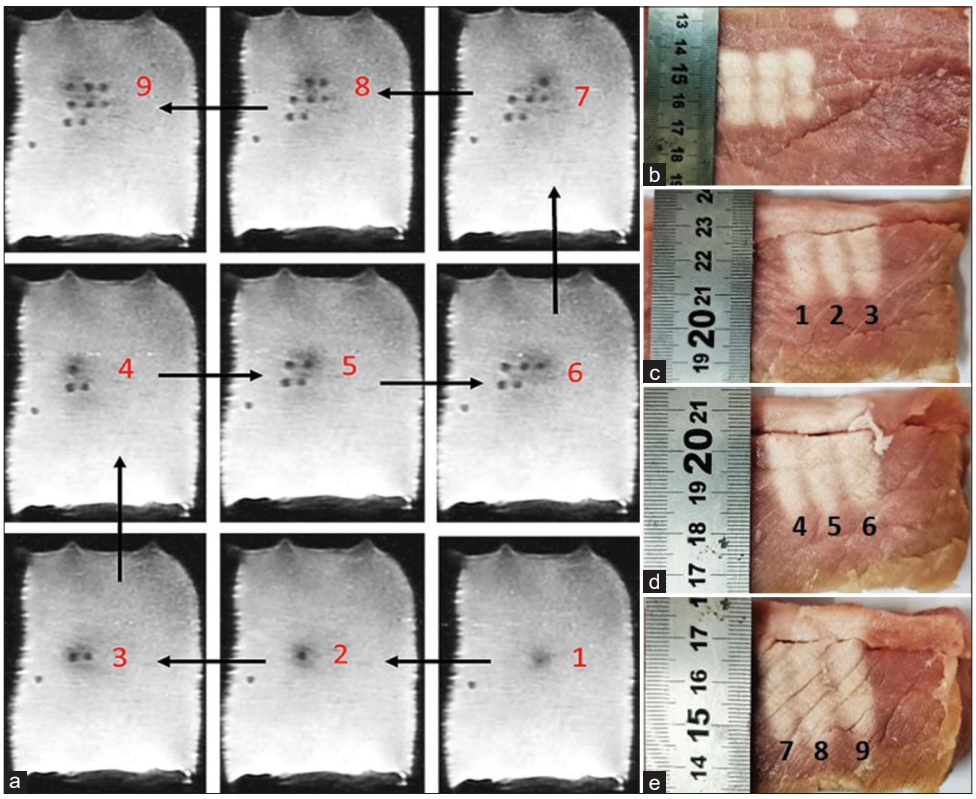

Figure 8: (a) 2D coronal T2-weighted fast spin echo images (repetition time = 2000 ms, echo time = 59 ms, flip angle = 90°, echo train length = 60, pixel bandwidth = 27.10 Hertz/pixel, matrix size = 224 × 192, field of view = 260 mm × 260 mm × 6 mm, and number of averages = 2) acquired during ablation in a 3 × 3 pattern (acoustical power of 54 W for 120, 10-mm step, 60-s delay) in the 1.5 T magnetic resonance imaging scanner. (b) The meat sliced (horizontally) at 10 mm from the sonicated side showing the formed lesions and the reference point lesion. (c-e) Photos of the tissue sliced vertically to assess the extent of necrosis in a plane parallel to the ultrasonic beam propagation: Lesions 1–3 had a length of 29 mm, lesions 4–6 a length of 30 mm, and lesions 7–9 a length of 32 mm

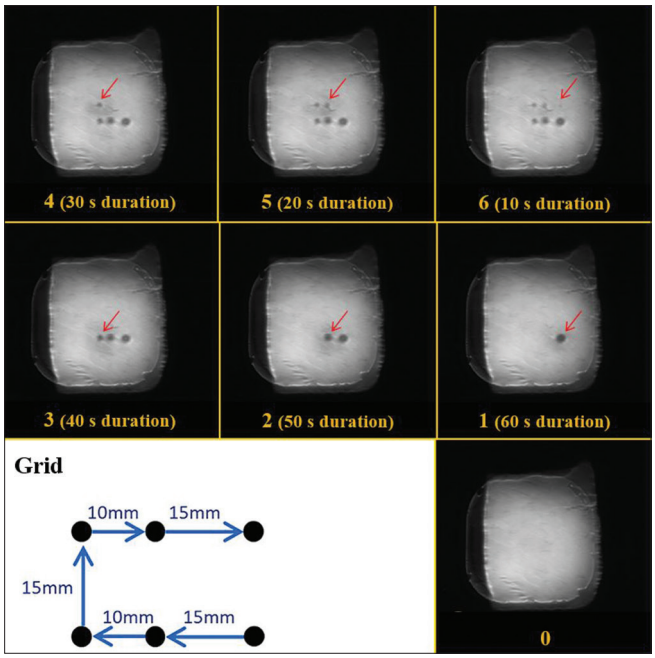

Figure 9: 2D coronal T2-weighted fast spin echo images (repetition time = 2500 ms, echo time = 48 ms, flip angle = 180°, echo train length = 60, PB = 50 Hz/pixel, matrix size = 256 × 256, and field of view = 200 mm × 200 mm × 10 mm) acquired during sonication in a 2 × 3 grid (acoustic power of 60 W) using varying sonication times and spatial step in the 3 T magnetic resonance imaging scanner. The sonication pattern is presented in the left bottom corner

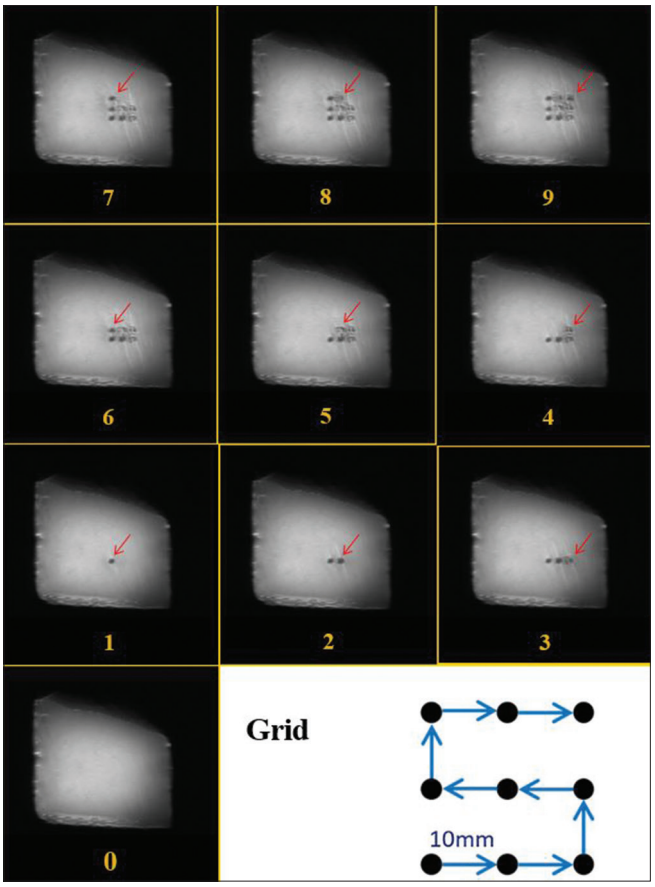

Figure 10: 2D coronal T2-weighted fast spin echo images (repetition time = 2500 ms, echo time = 48 ms, flip angle = 180°, echo train length = 60, PB = 50 Hz/pixel, matrix size = 256 × 256, and field of view = 200 mm × 200 mm × 10 mm) acquired during sonication in a 3 × 3 grid (acoustic power of 60 W for 40 s) with a spatial step of 10 mm (time delay of 60 s) in the 3 T magnetic resonance imaging scanner. The sonication pattern is presented in the right bottom corner

sample sonicated in a 2 × 3 grid with varying steps of 10 or 15 mm and sonication duration of 10–60 s, revealing the effect of sonication time on the resultant lesion size and distance between adjacent lesions. The T2-W FSE images of Figure 10 show the lesion progression for a 3 × 3 grid with a 10-mm step, where each spot was sonicated for 40 s. With the specific parameters, discrete lesions were inflicted in tissue. The T2-W FSE image of Figure 11a shows the overlapping lesion created by reducing the step to 5 mm while keeping the rest parameters identical. Figure 11b is a photo of a (horizontal) cross-section of the tissue sample at 10 mm from the top surface, revealing a rectangular necrotic area of about 20 mm × 20 mm.

Discussion

The present study provides parameter optimization on MRI monitoring of lesions produced by high-intensity FUS using T1-W and T2-W FSE sequences. Such sequences were widely employed for postsonication lesion assessment but not for intraprocedural monitoring of lesion progression during multiple ablations in grid patterns. A series of experiments were carried out in freshly excised porcine tissue to provide insights on this topic. Notably, excised porcine tissue is typically used in preclinical studies because it shares anatomical and physiological similarities with human tissue. It is considered a sufficiently representative preclinical model to obtain proof of concept and optimize newly proposed methodologies and applications before moving to *in vivo* studies. Furthermore, *ex vivo* animal tissue provides a controlled environment to assess feasibility without other factors (e.g., blood flow and motion of target) affecting the results.

The contrast in T1-W and T2-W FSE images arises from the variation in the longitudinal (T1) and transverse (T2) relaxation times among tissues.[25] It has been previously demonstrated that the relaxation times of FUS lesions and thus the contrast between healthy tissue and FUS lesions are strongly affected by the specific host tissue characteristic.[46-48] Herein, the FUS lesions were found as expected to possess lower T1 and T2 values than the surrounding nonsonicated porcine tissue at 3 T. This is consistent with what has been found in another study by Hadjisavvas *et al*.,[46] where lower T1 and T2 values were estimated for thermal lesions in *in vivo* rabbit kidney, liver, heart, and brain compared to the corresponding host tissue. Contrary to these findings, Eranki *et al*.[47] report that FUS lesions inflicted in *ex vivo* porcine liver, kidney, and cardiac muscle tissues appeared hyperintense in T2-W images with T2 values noticeably greater than the adjacent, untreated tissue.[47] However, this appears to be a case of

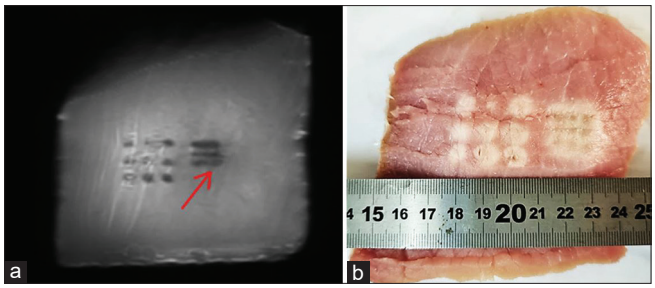

Figure 11: (a) 2D coronal T2-weighted fast spin echo image (repetition time = 2500 ms, echo time = 48 ms, flip angle = 180°, echo train length = 60, PB = 50 Hz/pixel, matrix size = 256 × 256, and field of view = 200 mm × 200 mm × 10 mm) acquired after sonication in a 3 × 3 grid (acoustic power of 60 W for 40 s) with a spatial step of 5 mm (time delay of 60 s) in the 3 T magnetic resonance imaging scanner. The red arrow indicates the formed overlapping lesion. The discrete lesion created with the 10-mm step is also visible on the left side. (b) Photo of the tissue sample cut horizontally at 10 mm from the sonicated surface

cavitation lesions as confirmed by previous research showing that thermal lesions produced by FUS appear hypointense in T2-W FSE images, whereas hyperintensity is associated with tissue boiling.[22] Opposite behavior is observed in the case of T1-W FSE imaging.[22] Therefore, the hypointense appearance of lesions on T2-W FSE images in the current study provides clear evidence of lesion creation by thermal mechanisms.

The study findings further suggest that the difference in MR relaxation properties between damaged and intact porcine tissues allows excellent lesion discrimination using T1-W and T2-W FSE sequences, provided that appropriate imaging parameters are employed. In this regard, a series of scans with varying parameters were performed to assess how the contrast between ablated and normal tissues is affected. For this purpose, a piece of porcine meat was sonicated using the 2.6 MHz FUS transducer using 68 W acoustic power for 120 s. The ETL, TE, and TR were the sequence parameters tested in terms of the CNR and acquisition time. Overall, higher CNR was achieved with the T2-W FSE sequence. It was thus concluded that T2-W FSE imaging is preferred for lesion monitoring in dead tissue, whereas in the case of live animals, T1-W imaging may be preferred due to the use of contrast agents.

CNR values above 80 were deemed sufficient for ease of detectability and proper visualization of FUS lesions. With the T1-W FSE sequence, CNR values above 80 were achieved for ETL values of up to 60 [Figure 3], with the value of 60 offering sufficiently high CNR at the minimum time cost (9 s). Therefore, considering both parameters, an ETL of 60 is suggested as the optimum.

The corresponding results on the effect of TR [Figure 4] reveal that the ratio of CNR to the acquisition time in T1-W FSE imaging begins to increase with increasing TR up to 1500 ms and then becomes almost flat, while at TR longer than 2000 ms, it begins to decrease again. On the contrary, the CNR gradually increases from 20 to 140 as TR increases from 700 to 2500 ms, attributing to the increase in the SI difference between lesion and tissue. Notably, this trend is expected to be reversed as the TR is getting longer and the SI of lesion and tissue is reaching its maximum value. In general, while TR values close to 2500 ms may be considered ideal in terms of maximizing contrast, a value close to 1500 ms constitutes a wiser option in the case of intraoperative monitoring of lesion progression since it still provides good CNR (>80) at smaller acquisition time.

Regarding T2-W FSE imaging, the results [Figure 5] confirm that the use of longer ETL causes CNR decrease. Nevertheless, when the CNR is divided by the acquisition time, an increasing trend is observed owing to that the acquisition time and ETL are inversely proportional. By choosing an ETL value in the range of 25–60, acceptable CNR (>80) is achieved at a reasonable acquisition time (<20 s). Further increasing the ETL to reduce the time may result in poor contrast making lesion discrimination difficult or infeasible. Again, the ETL of 60 was deemed ideal for minimizing the acquisition time.

Concerning the effect of TE, the trend of CNR versus TE [Figure 6] begins to increase until it reaches its maximum value of about 170 at TE close to 50 ms and then gradually decreases. Since the imaging time is not affected by the chosen TE, it was concluded that the TE of 50 ms is ideal for lesion monitoring by T2-W FSE imaging and was adopted in follow-up experiments. Interestingly, TE values around 50 ms can be considered appropriate for imaging at 1.5 T as well. However, as expected, superior contrast was observed in the 3 T scanner, with an almost 4-fold increase in the CNR at the TE of 50 ms. This result ties well with previous studies wherein authors have suggested the use of TE values between 40 and 50 ms to maximize the contrast of thermal lesions on T2-W FSE images following *in vivo* rabbit experiments.[46]

Finally, the effect of the matrix size and NEX on the CNR was investigated using the optimized TR, TE, and ETL values. For both sequences, the minimum NEX of 1 provided excellent CNR and was considered optimum in terms of minimizing the acquisition time. As expected, increasing matrix size resulted in a better resolution and CNR drop simultaneously increasing the imaging time. The matrix size of 256 × 256 was deemed optimum providing both good CNR (>80) and CNR/acquisition time.

The feasibility of monitoring lesion progression during grid sonications was assessed at both 1.5 T and 3 T using T2-W FSE sequences. The FUS transducer was navigated by a positioning system in the horizontal plane to sonicate porcine tissue samples in grid patterns with varying ultrasonic and grid parameters. Navigation was initiated by registering the transducer's location relative to the target in the MRI coordinates and sonicating the meat at the reference location of the transducer. Lesion formation at the reference point was confirmed by T2-W FSE imaging providing evidence of efficient ultrasonic coupling. The sonication pattern was then executed with intraprocedural acquisition of T2-W FSE images that enabled assessment of lesions progression over time. The lesions appeared as circular black spots with

excellent contrast from the surrounding tissue. Notably, immediately after sonication, the tissue surrounding these black spots appeared as a less hypointense area indicating heat accumulation around the coagulated tissue, which returned to its normal intensity during tissue cooling through heat dissipation mechanisms [Figures 8 and 9]. Note also that circular focal beams constitute evidence of lesion formation by thermal mechanisms, while in the case of boiling lesions, the beam was shown to be distorted.[22]

An interesting observation made during lesion monitoring in the 1.5 T MRI scanner [Figure 8] is that while only 8 out of the 9 sonicated spots showed clear evidence of lesion formation on the series of T2-W FSE images, 9 well-defined lesions were visualized following tissue dissection. In fact, a circular hypoenhanced area was observed immediately after the first sonication revealing heat accumulation in the relevant ROI, but it was not present in the next acquisitions [Figure 8a]. Tissue dissection revealed that the lesion had been shifted from the tissue surface and could only be detected if a deeper slice had been selected. It was also observed that the length of the formed lesions varied from 29 to 32 mm, most probably attributed to heat dissipation from previously sonicated spots [Figure 8c-e].

The excellent lesion contrast from the surrounding hyperintense background also allowed the assessment of the lesion size depending on the applied acoustic energy. In Figure 9, the spots of a 2 × 3 grid were sequentially exposed at similar acoustic power while the sonication time was decreased from 60 to 10 s resulting in lesions of decreasing diameter, with the last one receiving the lowest energy being barely visible. Furthermore, by varying the spatial step between sequential sonications, the distance between adjacent lesions on the T2-W FSE images was varied accordingly.

Lesion progression in both discrete and overlapping patterns was successfully monitored in the 3 T MRI scanner. When the grid spacing was reduced from 10 to 5 mm, while keeping the sonication parameters (acoustic power of 60 W, sonication time of 40 s) and time delay (60 s) constant, overlapping lesions were created [Figure 11]. In that case, the acquired images revealed a well-defined square area of reduced intensity [Figure 11a] that coincided well with the planned sonication pattern and actual overlapping lesion observed on tissue [Figure 11b].

Despite the very promising outcomes of the current study, when it comes to clinical usefulness, the use of *ex vivo* animal tissue has essential limitations compared to *in vivo* models, among which the absence of blood flow and motion is likely the most crucial. These two factors constitute important considerations when transitioning from *ex vivo* to *in vivo* studies and can both influence the applicability of our findings in a clinical setting.

As mentioned above, T2-W FSE imaging offered higher SNR and was considered more suitable for lesion monitoring in dead tissue, whereas in the case of live animals, T1-W imaging may be preferred due to the use of contrast agents. In general, for lesion localization and the assessment of basic tissue changes, T2-W FSE imaging will probably suffice in the *in vivo* scenario as well. However, contrast-enhanced T1-W imaging can provide additional insights about tissue dynamics and specifically changes in tissue perfusion. Furthermore, in an *in vivo* scenario, the accuracy of ultrasonic delivery and lesion monitoring may be significantly affected by tissue motion (e.g., respiration), potentially causing both shifting and inaccurate localization of lesions. However, this issue exists regardless of the monitoring method employed. Common strategies used to mitigate tissue movement effects, such as immobilization techniques and gating,[49] could be theoretically applied with the proposed technique as well.

Therefore, *in vivo* studies will be needed to demonstrate the clinical potential, especially for challenging organs, such as liver and kidney. Notably, *in vivo* application will require careful adjustment of the imaging techniques and experimental design to account for the aforementioned differences between *ex vivo* and *in vivo* conditions, as well as re-optimization of the imaging parameters for optimal CNR.

Conclusion

Overall, the current study provides insights on the topic of FUS lesion progression monitoring by T1-W and T2-W FSE imaging through a series of ablation experiments in *ex vivo* porcine tissue. The study findings confirmed that lesion discrimination on T1-W and T2-W FSE images highly depends on the selected MRI parameters, while the imaging time should also be considered in the context of intraprocedural lesion monitoring. Thereby, critical MR parameters, i.e. TE, TR, and ETL, should be optimized by balancing between the CNR and acquisition time. In this regard, the use of CNR values above 80 was set as the criterion for proper lesion visualization. Furthermore, considering the need to minimize the acquisition time, a TR close to 1500 ms is suggested for T1-W FSE imaging. A TE close to 50 ms was considered optimum for T2-W FSE imaging. For both sequences, an ETL of 60 was proven ideal. During sonications in discrete and overlapping patterns, acute FUS lesions were visualized as spots of reduced intensity on T2-W FSE images with excellent contrast from the surrounding intact tissue. It was demonstrated that multiple images should be acquired at varying depths in tissue to avoid nondetectability of shifted lesions, which constitutes a common phenomenon attributing to tissue inhomogeneities and/or the presence of bubbles that disturb the propagation of ultrasonic waves.

Financial support and sponsorship

The study was co-funded by the European Structural and Investment Funds (ESIF), Recovery and Resilience Plan of the European Union, and the Republic of Cyprus through the Research and Innovation Foundation (RIF). The robotic device used for the purposes of the study was developed under the project FUSROBOT (ENTERPRISES/0618/0016), whereas the reported experiments were carried out under the projects SOUNDPET (INTEGRATED/0918/0008) and FUSVET (SEED/1221/0080).

Conflicts of interest

There are no conflicts of interest.

References

1. Knavel EM, Brace CL. Tumor ablation: Common modalities and general practices. Tech Vasc Interv Radiol 2013;16:192-200.
2. Mellal I, Oukaira A, Kengene E, Lakhssassi A. Thermal therapy modalities for cancer treatment: A review and future perspectives. Int J Appl Sci Res Rev 2017;4:1-11.
3. Tinguely P, Paolucci I, Ruiter SJ, Weber S, de Jong KP, Candinas D, *et al.* Stereotactic and robotic minimally invasive thermal ablation of malignant liver tumors: A systematic review and meta-analysis. Front Oncol 2021;11:713685.
4. Yiallouras C, Damianou C. Review of MRI positioning devices for guiding focused ultrasound systems. Int J Med Robot 2015;11:247-55.
5. Mortele KJ, Silverman SG, Cantisani V, Tuncali K, Shankar S, Van Sonnenberg E. Magnetic resonance imaging guidance for tumor ablation. In: Van Sonnenberg E, McMullen WN, Solbiati L, Livraghi T, McMullen W, Solbiati L, Van Sonnenberg E, editors. Tumor Ablation: Principles and Practise. New York, NY: Springer; 2005. p. 148-66.
6. Lee EJ, Fomenko A, Lozano AM. Magnetic resonance-guided focused ultrasound: Current status and future perspectives in thermal ablation and blood-brain barrier opening. J Korean Neurosurg Soc 2019;62:10-26.
7. Zhu M, Sun Z, Ng CK. Image-guided thermal ablation with MR-based thermometry. Quant Imaging Med Surg 2017;7:356-68.
8. Fite BZ, Wang J, Ghanouni P, Ferrara KW. A review of imaging methods to assess ultrasound-mediated ablation. BME Front 2022;2022:9758652.
9. Kurose J, Kiuchi K, Fukuzawa K, Takami M, Mori S, Suehiro H, *et al.* Lesion characteristics between cryoballoon ablation and radiofrequency ablation with a contact force-sensing catheter: Late-gadolinium enhancement magnetic resonance imaging assessment. J Cardiovasc Electrophysiol 2020;31:2572-81.
10. Mont L, Roca-Luque I, Althoff TF. Ablation lesion assessment with MRI. Arrhythm Electrophysiol Rev 2022;11:e02.
11. Zhi-Yu H, Ping L, Xiao-Ling Y, Zhi-Gang C, Fang-Yi L, Jie Y. A clinical study of thermal monitoring techniques of ultrasound-guided microwave ablation for hepatocellular carcinoma in high-risk locations. Sci Rep 2017;7:41246.
12. Cline HE, Schenck JF, Watkins RD, Hynynen K, Jolesz FA. Magnetic resonance-guided thermal surgery. Magn Reson Med 1993;30:98-106.
13. Hynynen K, Freund WR, Cline HE, Chung AH, Watkins RD, Vetro JP, *et al*. A clinical, noninvasive, MR imaging-monitored ultrasound surgery method. Radiographics 1996;16:185-95.
14. Hynynen K, Darkazanli A, Unger E, Schenck JF. MRI-guided noninvasive ultrasound surgery. Med Phys 1993;20:107-15.
15. Hynynen K, Darkazanli A, Damianou CA, Unger E, Schenck JF. The usefulness of a contrast agent and gradient-recalled acquisition in a steady-state imaging sequence for magnetic resonance imaging-guided noninvasive ultrasound surgery. Invest Radiol 1994;29:897-903.
16. Chung AH, Jolesz FA, Hynynen K. Thermal dosimetry of a focused ultrasound beam *in vivo* by magnetic resonance imaging. Med Phys 1999;26:2017-26.
17. Chen L, Bouley D, Yuh E, D'Arceuil H, Butts K. Study of focused ultrasound tissue damage using MRI and histology. J Magn Reson Imaging 1999;10:146-53.
18. Foldes K, Hynynen K, Shortkroff S, Winalski CS, Collucci V, Koskinen SK, *et al.* Magnetic resonance imaging-guided focused ultrasound synovectomy. Scand J Rheumatol 1999;28:233-7.
19. Vykhodtseva N, Sorrentino V, Jolesz FA, Bronson RT, Hynynen K. MRI detection of the thermal effects of focused ultrasound on the brain. Ultrasound Med Biol 2000;26:871-80.
20. Curiel L, Souchon R, Rouvière O, Gelet A, Chapelon JY. Elastography for the follow-up of high-intensity focused ultrasound prostate cancer treatment: Initial comparison with MRI. Ultrasound Med Biol 2005;31:1461-8.
21. Rivens I, Shaw A, Civale J, Morris H. Treatment monitoring and thermometry for therapeutic focused ultrasound. Int J Hyperthermia 2007;23:121-39.
22. Damianou C, Ioannides K, Hadjisavvas V, Mylonas N, Couppis A, Iosif D. MRI monitoring of lesions created at temperature below the boiling point and of lesions created above the boiling point using high intensity focused ultrasound. J Biomed Sci Eng 2010;3:763-75.
23. Damianou C, Ioannides K, Hadjisavvas V, Mylonas N, Couppis A, Iosif D. *In vitro* and *in vivo* brain ablation created by high-intensity focused ultrasound and monitored by MRI. IEEE Trans Ultrason Ferroelectr Freq Control 2009;56:1189-98.
24. Celik H, Ramanan V, Barry J, Ghate S, Leber V, Oduneye S, *et al.* Intrinsic contrast for characterization of acute radiofrequency ablation lesions. Circ Arrhythm Electrophysiol 2014;7:718-27.
25. Rieke V, Butts Pauly K. MR thermometry. J Magn Reson Imaging 2008;27:376-90.
26. Bremer C, Kreft G, Filler T, Reimer P. Accuracy of non-enhanced MRI to monitor histological lesion size during laser-induced interstitial thermotherapy. Eur Radiol 2002;12:237-44.
27. Vergara GR, Vijayakumar S, Kholmovski EG, Blauer JJ, Guttman MA, Gloschat C, *et al.* Real-time magnetic resonance imaging-guided radiofrequency atrial ablation and visualization of lesion formation at 3 tesla. Heart Rhythm 2011;8:295-303.
28. Nordbeck P, Hiller KH, Fidler F, Warmuth M, Burkard N, Nahrendorf M, *et al.* Feasibility of contrast-enhanced and nonenhanced MRI for intraprocedural and postprocedural lesion visualization in interventional electrophysiology: Animal studies and early delineation of isthmus ablation lesions in patients with typical atrial flutter. Circ Cardiovasc Imaging 2011;4:282-94.
29. Lin Z, Chen J, Yan Y, Chen J, Li Y. Microwave ablation of hepatic malignant tumors using 1.5T MRI guidance and monitoring: Feasibility and preliminary clinical experience. Int J Hyperthermia 2019;36:1216-22.
30. Izadifar Z, Izadifar Z, Chapman D, Babyn P. An introduction to high intensity focused ultrasound: Systematic review on principles, devices, and clinical applications. J Clin Med 2020;9:460.
31. Antoniou A, Giannakou M, Evripidou N, Evripidou G, Spanoudes K, Menikou G, *et al.* Robotic system for magnetic resonance guided focused ultrasound ablation of abdominal cancer. Int J Med Robot 2021;17:e2299.
32. Antoniou A, Giannakou M, Evripidou N, Stratis S, Pichardo S, Damianou C. Robotic system for top to bottom MRgFUS therapy of multiple cancer types. Int J Med Robot 2022;18:e2364.
33. Epaminonda E, Drakos T, Kalogirou C, Theodoulou M, Yiallouras C, Damianou C. MRI guided focused ultrasound robotic system for the treatment of gynaecological tumors. Int J Med Robot 2016;12:46-52.
34. Giannakou M, Yiallouras C, Menikou G, Ioannides C, Damianou C. MRI-guided frameless biopsy robotic system with the inclusion of unfocused ultrasound transducer for brain cancer ablation. Int J Med Robot 2019;15:e1951.
35. Menikou G, Yiallouras C, Yiannakou M, Damianou C. MRI-guided focused ultrasound robotic system for the treatment of bone cancer. Int J Med Robot 2017;13:1-11. [doi: 10.1002/rcs. 1753].
36. Yiannakou M, Menikou G, Yiallouras C, Ioannides C, Damianou C. MRI guided focused ultrasound robotic system for animal experiments. Int J Med Robot 2017;13:e1804. [doi: 10.1002/rcs. 1804].
37. Antoniou A, Giannakou M, Georgiou E, Kleopa KA, Damianou C. Robotic device for transcranial focussed ultrasound applications in small animal models. Int J Med Robot 2022;18:e2447.
38. Giannakou M, Antoniou A, Damianou C. Preclinical robotic device for magnetic resonance imaging guided focussed ultrasound. Int J Med Robot 2023;19:e2466.
39. Allen SP, Prada F, Xu Z, Gatesman J, Feng X, Sporkin H, *et al.* A preclinical study of diffusion-weighted MRI contrast as an early indicator of thermal ablation. Magn Reson Med 2021;85:2145-59.
40. Drakos T, Giannakou M, Menikou G, Filippou A, Evripidou N, Spanoudes K. MRI-guided focused ultrasound robotic system for preclinical use. J Vet Med Anim Sci 2021;4:1-11.
41. Antoniou A, Georgiou L, Evripidou N, Ioannides C, Damianou C. Challenges regarding MR compatibility of an MRgFUS robotic system. J Magn Reson 2022;344:107317.
42. Liberman G, Louzoun Y, Ben Bashat D. T mapping using variable flip

angle SPGR data with flip angle correction. J Magn Reson Imaging 2014;40:171-80.
43. Bojorquez JZ, Bricq S, Acquitter C, Brunotte F, Walker PM, Lalande A. What are normal relaxation times of tissues at 3 T? Magn Reson Imaging 2017;35:69-80.
44. Hendrick RE. Signal, noise, signal-to-noise, and contrast-to-noise ratios. In: Breast MRI: Fundamentals and Technical Aspects. New York, NY: Springer New York; 2008. p. 107-10.
45. Filippou A, Drakos T, Giannakou M, Evripidou N, Damianou C. Experimental evaluation of the near-field and far-field heating of focused ultrasound using the thermal dose concept. Ultrasonics 2021;116:106513.
46. Hadjisavvas V, Ioannides K, Komodromos M, Mylonas N, Damianou C. Evaluation of the contrast between tissues and thermal lesions in rabbit *in vivo* produced by high intensity focused ultrasound using fast spin echo MRI sequences. J Biomed Sci Eng 2010;4:51-61.
47. Eranki A, Farr N, Partanen A, Sharma KV, Rossi CT, Rosenberg AZ, *et al.* Mechanical fractionation of tissues using microsecond-long HIFU pulses on a clinical MR-HIFU system. Int J Hyperthermia 2018;34:1213-24.
48. Kholmovski E, Ranjan R, Angel N, Marrouche NF. T2*-weighted MRI technique for visualization of RF ablation lesions. J Cardiovasc Magn Reson 2016;18 Suppl 1:2-4.
49. Schlesinger D, Benedict S, Diederich C, Gedroyc W, Klibanov A, Larner J. MR-guided focused ultrasound surgery, present and future. Med Phys 2013;40:080901.